Proceedings of ASME 2011 5th International Conference on Energy Sustainability & 9th Fuel Cell Science, Engineering and Technology Conference
ESFuelCell2011
August 7-10, 2011, Washington, DC, USA

ESFuelCell2011-54258

STAINLESS STEEL 316L AND INCONEL 625 MATERIAL COMPATIBILITY WITH PHASE CHANGE SALT FOR THERMAL ENERGY STORAGE SYSTEMS

Songgang Qiu, Ross Galbraith, Ming Fang
Infinia Technology Company
Kennewick, WA, USA

Brian D. Iverson
Sandia National Laboratories
Albuquerque, NM, USA

Bradley Ring
U.S. Department of Energy
Golden, CO, USA

Suzanne Baca
Navarro Research & Engineering, Inc.
Golden, CO, USA

ABSTRACT

Infinia Corporation is developing a 3 kW solar dish Free Piston Stirling Engine (FPSE) system to provide a scalable solar power solution that will enable broad access to inexpensive, mass-manufactured solar power. To balance the energy demand between day time and night time and to remedy cloud transients, a thermal energy storage (TES) system that is integrated with a modified version of Infinia's 3-kW solar dish FPSE system is being developed by Infinia Corporation under a U.S. Department of Energy contract. The thermal energy storage module contains a phase-change material (salt). This paper presents the results of a material compatibility study conducted to determine the suitability of Stainless Steel 316L and Inconel 625 alloys for use in the construction of the TES module. Sample containers made from the two materials were fabricated and filled with NaF/NaCl salt. The samples were then heated to a constant 750 °C. One each of the samples was removed at both 100 and 2500 hours' time. The containers were cut open to analyze the material surface and cross section. After 100 and 2500 hours, both materials exhibited a very little corrosion. Initially, the SS 316L suffered a shallow grain boundary attack, on the level of 1-2 microns in depth. The Inconel 625 formed an oxide complex, which is resistant to element dissolution into the molten salt. After 2500 hours, the surface morphology for both materials was largely unchanged, with the corrosion process having switched from an initial localized type, to a more uniform type. Both materials show promise of resistance to salt attack, although Inconel 625 appears to have a slight advantage.

INTRODUCTION

Infinia is developing a thermal energy storage (TES) system that is integrated with a modified version of Infinia's 3 kW solar dish Free Piston Stirling Engine (FPSE) system under a U.S. Department of Energy contract. Dish Stirling concentrating solar power (CSP) has been considered over the past 20 years to offer excellent prospects for large-scale production of cost-effective, high efficiency solar electric power [1,2]. Infinia's FPSE with unique flexure bearings and clearance seals, no wearing parts, and no lubricants, have been shown to have maintenance free design lives of 150,000 hours [3]. To provide electricity during cloud transients and non-daylight hours, Infinia is developing a TES module that contains a phase-change material (PCM) salt between the solar thermal receiver and the engine. The TES system uses PCM salts of high melting points to maximize energy storage density by utilizing both the latent heat and sensible heat over wide operating temperature ranges. The TES system was designed to provide sufficient thermal energy for additional 3 kWh of power production.

One challenge in the design of the TES system is with the selection of materials with which the salt vessel will be built. Key requirements include strength and corrosion resistance at elevated temperatures, raw material cost, commercial availability, and manufacturability using common fabrication methods. The PCM being used is an alkali halide salt; a NaF/NaCl eutectic mixture in an evacuated and hermetically sealed container. Sunlight from a mirrored parabolic dish concentrator is directed onto the receiver end of the TES module, where its thermal energy is transferred to the PCM via a system of high temperature heat pipes embedded in it. These heat pipes also serve to deliver the thermal energy to the

Stirling engine during PCM discharge. A picture of the TES module integrated with a 3 kW Stirling engine is shown in Figure 1. Due to variations in solar insolation throughout the day, the TES module is subjected to temperatures ranging from local ambient to 700 °C.

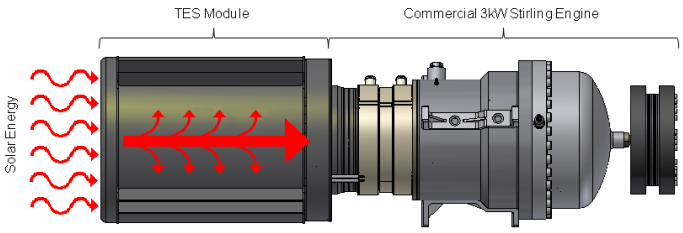

Figure 1 TES Module and 3 kW Stirling Engine Assembly

NOMENCLATURE

CSP	Concentrating Solar Power
EDX	Energy-Dispersive X-Ray Spectroscopy
FPSE	Free Piston Stirling Engine
PCM	Phase Change Material
SEM	Scanning Electron Microscopy
TES	Thermal Energy Storage

MATERIAL SELECTION

Use of molten salts can be found in three major technology fields: nuclear, air & space, and solar power generation. A literature review was conducted to assess the relevance of these applications to Infinia's TES system. The data and results from NASA's space program share the most similarity to this project because of the high operating temperatures, usage of alkali halide salts, and closed system operation. A down-select process for the TES container material to be used with alkali halide salts yielded five likely materials, from which, Stainless Steel 316L (SS 316L) and Inconel 625 were selected and tested due to availability and raw material cost. Although extensive compatibility work has been done with alkali fluoride salt mixtures in the past, no studies using a NaF/NaCl mixture were found. Given the salts' chemical similarities, earlier works served as a guide for material selection. The following points summarize some conclusions drawn from previous testing with alkali fluoride salts.

- Current commercially available high temperature alloys can serve as the salt container. In particular, Inconel 617 and SS 304 have been reported to have very limited degradation with no signs of failure after 5 years of thermal cycling.
- Three oxidizing agents are found in the salt system: O_2 and H_2O residue, and Na cations.
- With limited strong oxidizing agent availability, the corrosion rate of alloys in molten salt decrease over time.
- Minimizing O_2 and H_2O levels in the TES module is critical to hardware life. Catastrophic material failure due to corrosion can occur within a week when significant amounts of H_2O and O_2 are present in the system.
- Sodium cations are not predicted as an active oxidizer due to low electronegativity amongst all the elements in the material system.

The five types of alloys initially selected are shown in Table 1. Three of the materials – Incoloy 800HT, Inconel 617 and Hastelloy N - were eliminated from consideration due to high cost, low availability or difficulty with machining and/or welding.

Table 1 TES vessel material candidates

Name	Alloy	Ni	Fe+Cr	$ rank
SS 316L	SS	Low	High	Low
Incoloy 800HT	Fe-Ni	↓	↑	↓
Inconel617	Ni-Cr			
Inconel 625	Ni-Cr			
Hastelloy N	Hi Ni	High	Low	High

SAMPLE PREPARATION AND TESTING

Cylindrical containers of approximately 35 cm^3 interior volume were fabricated from both SS 316L and Inconel 625 as illustrated in Figure 2. In order to avoid sample contamination, electron beam welding was used to join the end caps to the cylindrical body as well as the fill tube to the assembled container. Salt is introduced into the container by way of a small fill tube, which is later crimped and sealed by fusion welding.

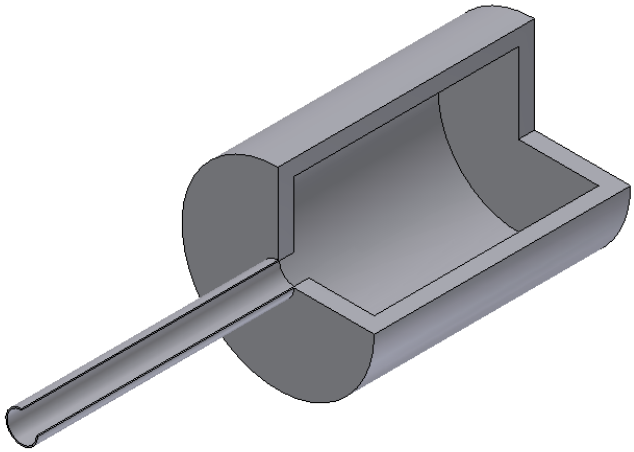

Figure 2 Test sample container

The sample containers are cleaned by ultrasonic agitation first in solvent, followed by deionized water. The containers are dried by nitrogen blow, and subjected to a low temperature bake-out in an oven at atmospheric conditions for 3 hours at 200 °C and then in an evacuated oven at 1.6×10^{-4} Torr for 4 hours at 400 °C. The salt constituents are also baked on a hotplate at 200 °C for 10 hours in a glove box to drive off excess O_2 and H_2O contaminants prior to filling. A eutectic mixture of NaF/NaCl salt at 4N (99.99% purity) grade is used

to fill the container while in the glove box, taking into account the volume change upon melting. The environmentally controlled glove box provided conditions of O_2<10 ppm and H_2O<10 ppm. After filling, the container is pumped down to 10^{-6} Torr and the fill tube pinched by a hydraulic crimping tool. The fill tube is then cut and sealed across the crimp using a fusion weld.

Multiple samples of SS 316L and Inconel 625 were placed in an oven held at a constant 750 °C; 70 degrees above the eutectic melting point of NaF/NaCl. The samples are exposed to ambient pressure conditions on the sample container exterior, while the interior contains the salt under vacuum at 10^{-6} Torr. After the samples were baked at temperature for 100 or 2500 hours, the samples were removed from the oven and sectioned for interrogation.

RESULTS AND ANALYSIS

One each of the SS 316L and Inconel 625 samples was removed after heating for a period of 100 and 2500 hours. The samples were cut open, and the container surface and cross section analyzed using scanning electron microscopy (SEM) and energy-dispersive X-ray spectroscopy (EDX) techniques.

SS 316L, 100 hour Test

The sample for SEM characterization was taken from the side wall of the container near the blind end cap, including the weld area. The sample was attached to the holder with conductive adhesive tape, and coated with carbon. The SEM tool used is a Quanta 3D FEG by FEI Corp.

In order to establish a baseline for comparison, an unused sample container was first analyzed. As expected the surface was protected by a chromium oxide layer, and no corrosion was observed. A top surface EDX analysis revealed, however, an enrichment of manganese and copper. These two elements have the highest vapor pressures of the alloy constituents at elevated temperatures [4]. Therefore, it is possible that they preferentially evaporate during the weld process, and were re-deposited on to the surface when cooling. Figure 3 shows the surface morphology of the unused sample. The defects seen are machining marks.

Figure 4 shows the interior surface of a SS 316L sample after 100 hours of testing. The surface shows significant roughness after interaction with the molten salt. Polycrystalline grains and the grain boundaries are exposed. Corrosion sites feature a shallow, "V"-shaped groove and a homogeneous surface roughness demonstrating that after corrosion is initiated, it progresses uniformly in all directions. This morphology further suggests that two types of localized metal dissolution have initiated: intergranular and pitting. The dissolution level varies considerably along grain boundaries, with the majority showing only slight amounts of corrosion. Also, the corrosion pits are observed to be located at grain boundary junctions, suggesting that all localized attack starts at the boundaries. Finally, there are no products of corrosion found on the sample substrate, indicating dissolution into the molten salt [5, 6].

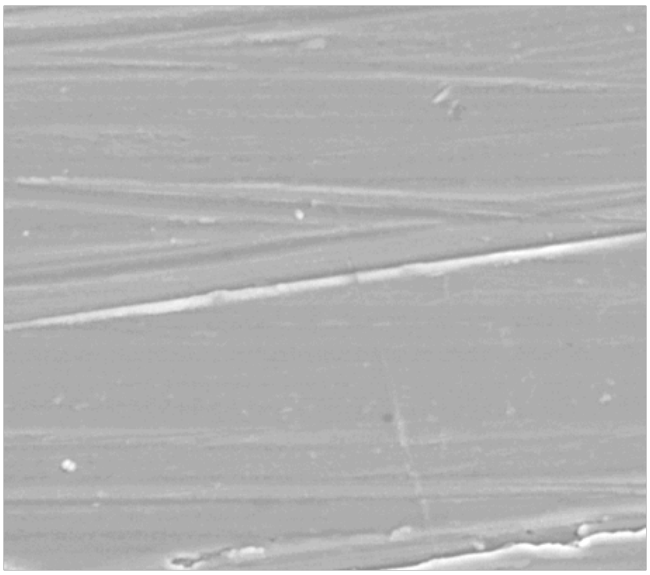

Figure 3 Top-down SEM image of SS 316L sample surface, untested (5000X)

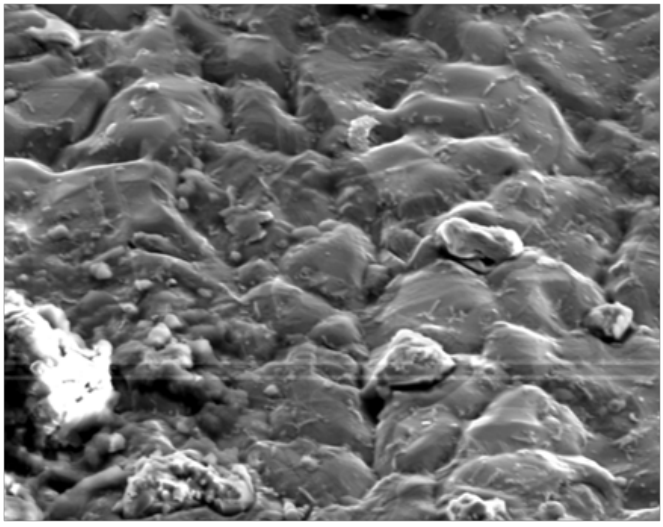

Figure 4 Tilted SEM image of SS 316L sample surface, 100 hours testing (5000X)

Four sites on the sample surface are selected for EDX chemical analysis, with the results shown in Table 2 below.

Table 2 EDX chemical analysis and resulting weight percentage of SS 316L sample surface, 100 hours testing

Site	O%	F%	Na%	Fe%	Cr%	Ni%	Mo%	Mn%
1	-	-	-	71	11.62	10.9	6	-
2	2.55	-	-	61	10.54	8.7	10.2	-
3	1.78	-	1.57	70	11.24	10.3	3	-
4	11	13.4	16.7	11.5	33.06	1.6	-	2.1

Surface oxide and salt particles are not evenly distributed on the sample surface. Site 1 exhibits undetectable levels of

oxygen, fluorine, and sodium indicative of an area free from salt and oxide. Sites 2 and 3 have varying small amounts of oxide and salt. Site 4 shows not only salt residue, but chromium enriched surface oxide. Also significant is the molybdenum enrichment at Sites 1 and 2, as well as the depletion of manganese at Sites 1 through 3.

A cross sectional view of the sample specimen is shown in Figure 5 below. Deep grain boundary corrosion penetration is not observed, and no visible micro-voids caused by element depletion are seen. Grain recrystallization and growth has occurred as a result of annealing, replacing the refined and severely distorted grains found in the untested sample due to machining cold work. This is a favorable result as the larger annealed grains are more stable, and therefore provide greater corrosion resistance than those that are deformed plastically.

EDX analysis was performed on the 100 hour, SS 316L sample cross section to characterize the concentration of key elements. This technique performed on the cross section is more accurate than that performed on the surface due to reduced interference from the surface oxide and salt contamination. The cross section was sampled at various locations along its depth, the results of which are shown in Figure 6. Surface depletion of chromium and enrichment of molybdenum are evident, while the concentration variations of iron and nickel are unremarkable. Chromium dissolution is a primary mechanism of corrosion in stainless steel, and it is shown to reach its nominal composition at a depth of approximately 6 microns. This dissolution of chromium into the salt occurs by two reaction paths. In the first instance, the chromium reacts with oxidants from residual O_2 and H_2O contaminates, forming surface chromium oxide. This oxide dissolves into the molten salt. The second reaction entails chromium carbide precipitation at the grain boundaries, which also dissolves into the salt.

In contrast to the reduction of chromium near the surface is the enrichment of molybdenum. Molybdenum has high diffusion mobility at elevated temperatures, and may be driven to the surface by the vacancies created by chromium depletion [7]. Molybdenum can also migrate to grain boundaries, forming carbides there.

The weld zone is the final area of study. Although electron beam welding was used in fabricating the sample container to avoid introducing contaminants, the welding process itself changes the material's microstructure, composition and properties. A cross section sample of SS316L in the weld zone is shown in Figure 7. The top of the image shows a layer several micron thick formed by metal overflow from the fusion pool, with a coating that results from metal vapor deposition. The vertical lines are artifacts from rough ion beam milling used during sample preparation. An interface boundary can be seen between the upper layer and the base metal, indicating incomplete fusion. There are also micro-voids present along or adjacent to the boundary.

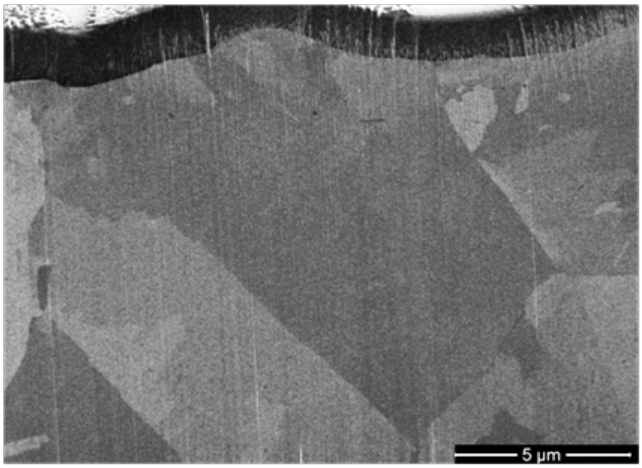

Figure 5. Cross section SEM image (12000x)

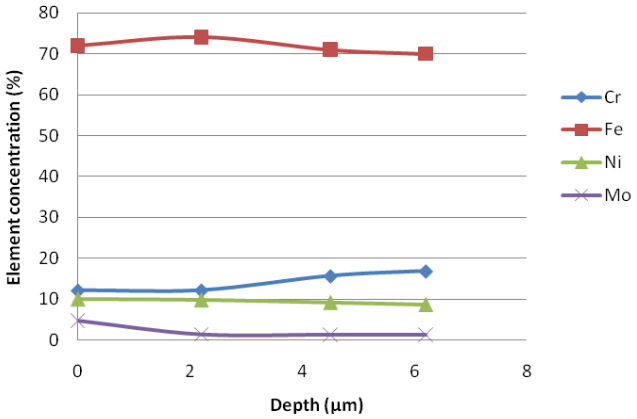

Figure 6 EDX chemical analysis of SS 316L sample at 100 hours testing

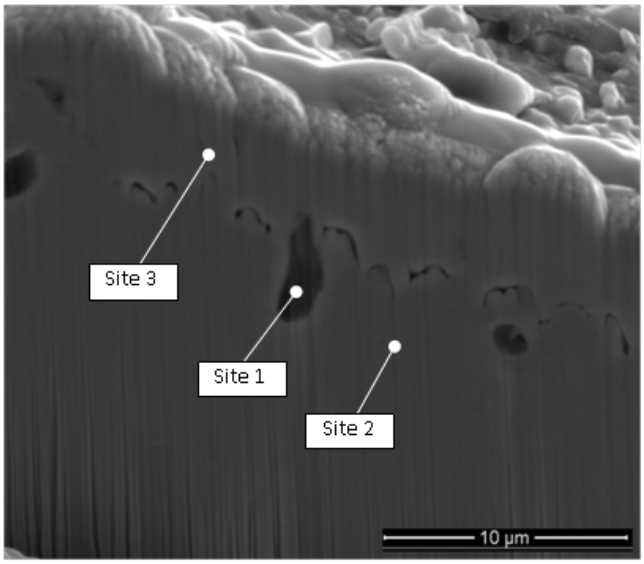

Figure 7 Cross section SEM image of SS 316L sample in the weld zone, 100 hours testing

Three sites were chosen on the cross section for EDX analysis: the largest void at center, the base material, and the top layer. These sites are labeled 1, 2 and 3 respectively, and are referenced in Table 3. In Site 1, there is a large percentage of both sodium and chlorine in the void, indicating the presence of salt. The salt could have fallen in from the wall surface during ion beam milling. It is also possible that the void is connected to the surface in contact with the salt via a grain boundary or micro-crack from the weld, allowing the intrusion of molten salt. Manganese depletion is evident in each sample site, again suggesting that this high vapor pressure element evaporates during the welding process, later depositing on the surface.

Table 3 EDX chemical analysis and resulting weight percentage of SS 316L sample in the weld zone, 100 hours testing

Site	O%	Cl%	Na%	Fe%	Cr%	Ni%	Mo%	Mn%
1	1.7	20.5	10.5	50	15.2	9.6	1.6	0.5
2	1.1	-	-	70.1	17.1	8.7	1.5	1.0
3	1.4	0.3	-	71	11.24	9.1	3	0.7

SS 316L, 2500 hours

The surface morphology (Figure 8) of a sample analyzed after 2500 hours testing indicates that a uniform metal dissolution process occurred after 100 hours. No significant intergranular corrosion developed, however more pits located at grain boundary junctions and shallow pits within the grains themselves are evident. Another observation is that some grain facets are exposed as a result of preferential dissolution of certain crystal orientations. The characterizations above suggest a shift in corrosion mechanism between 100 and 2500 hours' exposure to molten salt. After an initial intergranular boundary attack, the corrosion becomes much more uniform on a macro-scale.

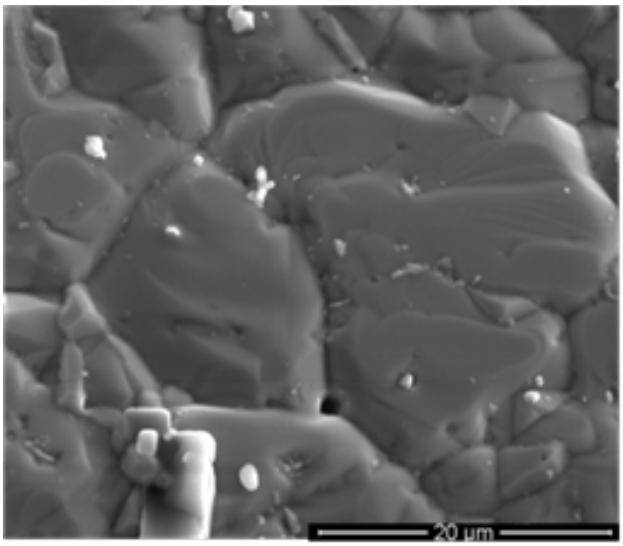

Figure 8 Top-down SEM image of SS 316L sample surface, 2500 hours testing (5000X)

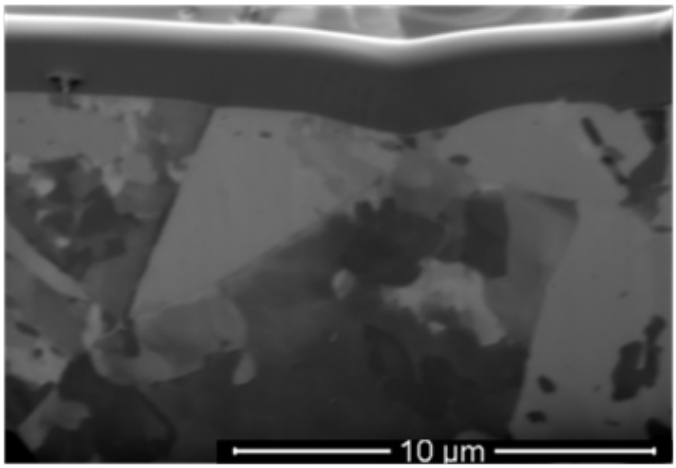

(a)

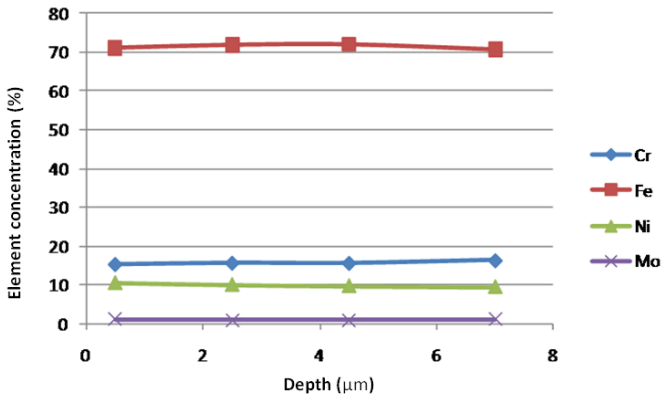

(b)

Figure 9 (a) Cross section SEM image (10000x) and (b) EDX chemical analysis of SS 316L sample at 2500 hours testing

A higher resolution, cross sectional image, shown in Figure 9a, supports the above conclusion in that no intergranular penetration is apparent. A top down surface EDX analysis was not conducted but the more accurate cross section survey was performed and the results are shown in Figure 9b. As before, locations along the sample's depth were tested for concentrations of key elements. Compared to the previous result at 100 hours, the elements' variation as a function of depth is much less pronounced, because the elements have had sufficient time to migrate to equilibrium concentrations within the material.

The weld zone cross section was also analyzed by SEM. The distinct fusion pool layer and micro-voids found in the 100 hours testing sample are not observed in multiple weld zone locations within the sample. The cause for this is unknown. However, one possible explanation is that the sample suffered corrosion at the interface boundary between the fusion pool and base metal layers. The thin fusion pool layer could then de-laminate from the material surface.

Inconel 625, 100 hours

An untested container was analyzed for a baseline comparison to the tested samples. SEM images of both the top-down surface and cross section reveal machining marks and grain refinement and distortion as a result of cold working, similar to that of the SS 316L. However, a top-down and cross sectional EDX analysis demonstrates that no elements on the surface deviate from the nominal composition of the bulk alloy. Both material type sample containers were electron beam welded using the same equipment and process parameters, yet the welding did not produce copper and manganese enriched thin films as with the stainless steel. Inconel 625 is composed primarily of elements with a high melting temperature and low vapor pressure. Its copper and manganese content are 0.02% and 0.03% by weight respectively; which are one to two orders of magnitude lower than the composition of SS 316L. It is apparent that these high vapor pressure elements do not experience significant evaporation during the welding process.

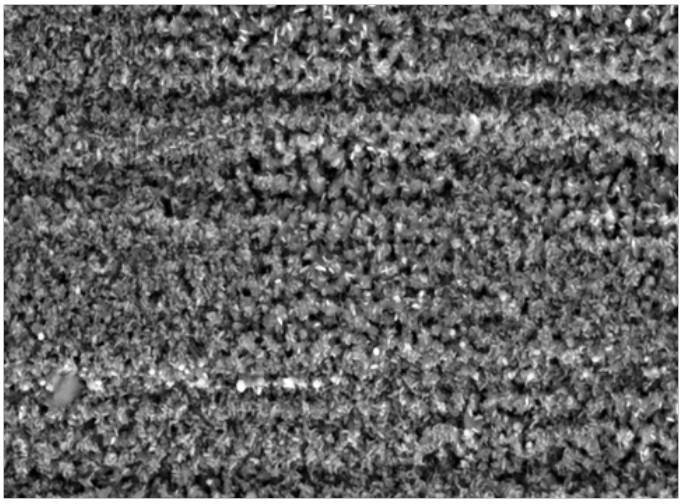

Figure 10 Top down SEM image of Inconel 625 sample surface, 100 hours testing (5000X)

After 100 hours of exposure to the molten salt, the surface morphology of the Inconel 625 is significantly different than that of the stainless steel. The Inconel 625 sample surface was evenly covered by oxide and salt residue. To assist in the evaluation, the sample was cleaned using ultrasonic agitation in a de-ionized water bath. Figure 10 shows the sample surface after cleaning. The surface is uniformly covered by an oxide layer of approximately 0.5 μm in thickness. The formation of each oxide is a grain of a few hundred nm in size. The oxide grains agglomerate and form a dense layer, although there are gaps between grains permitting the intrusion of molten salt.

In contrast to the stainless steel surface oxide which readily dissolves in the molten salt, the oxide complex that forms on Inconel 625 is stable and resistant to dissolution. A top-down EDX surface analysis at a single location was conducted, the result of which is shown in Table 4 using atomic percentage. Clearly, the resulting oxide complex is not in the form of Cr_2O_3, based on these atomic percentages. While, the oxide complex is rich in chromium and nickel the exact composition cannot be found by EDX analysis alone, and has not been determined.

Table 4 EDX chemical analysis and resulting atomic percentage of Inconel 625 sample surface, 100 hours testing

Element	O	Na	Cr	Fe	Ni	Mo
Atomic %	31	0.25	49	0.6	21.5	1.5

Figure 11 provides micro-structural view of the Inconel at its cross section. The top surface grains are significantly smaller than those found deeper within the sample. In addition, the large grains are found to contain annealing twins formed by recrystallization. Precipitates are also visible on the grain boundaries of the upper layer grains. These precipitates have a hindering effect on grain boundary mobility, and thus retard recrystallization and growth at the surface [8].

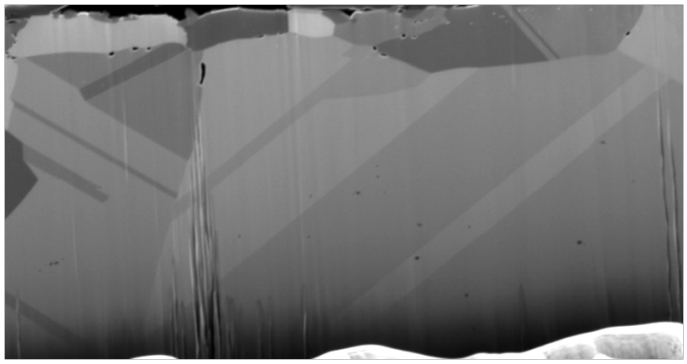

Figure 11 Cross section SEM image of Inconel 625 sample, 100 hours testing (10000X)

A number of sites for EDX cross sectional analysis are chosen. Site 1 is located within the oxide layer, Sites 2 and 3 are located at grain boundaries/precipitates, and Site 4 is located within the base material. The EDX results are shown in Table 5 below. Site 1 results validate the existence of high chromium content oxide seen in the surface analysis. Sites 2 and 3 suggest the presence of aluminum oxide precipitates, while Site 4 provides a comparison to the baseline composition. One element of the salt eutectic, sodium is not found in any concentration at the selected sites.

Table 5 EDX chemical analysis and resulting weight percentage of Inconel 625 sample cross section, 100 hours testing

Site	O%	Na%	Al%	Cl%	Cr%	Mn%	Fe%	Ni%	Mo%
1	12.9	-	-	-	53.2	-	1	31.7	2.8
2	3.9	-	4.4	-	18	0.1	1.7	67.9	4.4
3	3.7	-	3.1	0.2	18.6	0.16	1.7	68	4.6
4	0.35	-	-	-	18.2	0.1	1.7	74.6	5.1

Inconel 625, 2500 hours

The Inconel sample at 2500 hours was cleaned as before to remove salt residue prior to SEM analysis. The surface morphology seen in Figure 12 below is very similar to the sample at 100 hours of testing. The porous polycrystalline oxide layer is present, with no noticeable change in either grain size or thickness. This provides confirmation that the oxide complex is resistant to dissolution in the salt eutectic.

A cross section (Figure 13) SEM analysis validates the conclusions drawn from the surface study. The size of the oxide grains and thickness of the oxide layer indicate very little development with increased testing time. It is also observed that there is no evident undercut corrosion attack between the oxide layer and the alloy surface. In addition, there is limited intergranular boundary attack activity found. Some micron or sub-micron size voids are seen, which is likely the result of corrosion due to material defects in the manufacturing process.

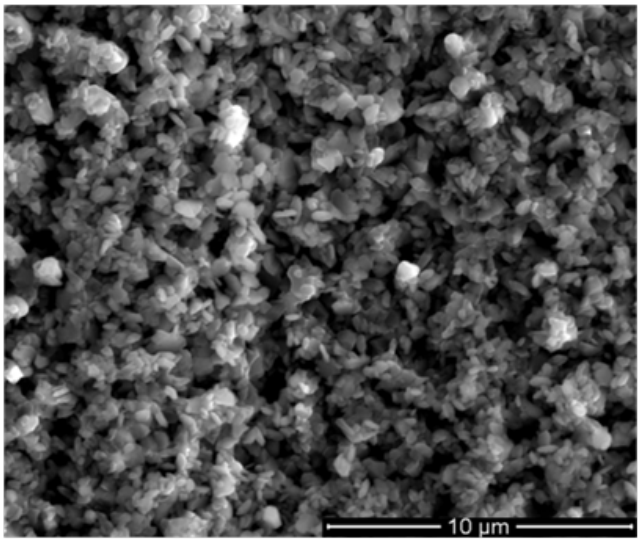

Figure 12 Top down SEM image of Inconel 625 sample surface, 2500 hours testing (10000X)

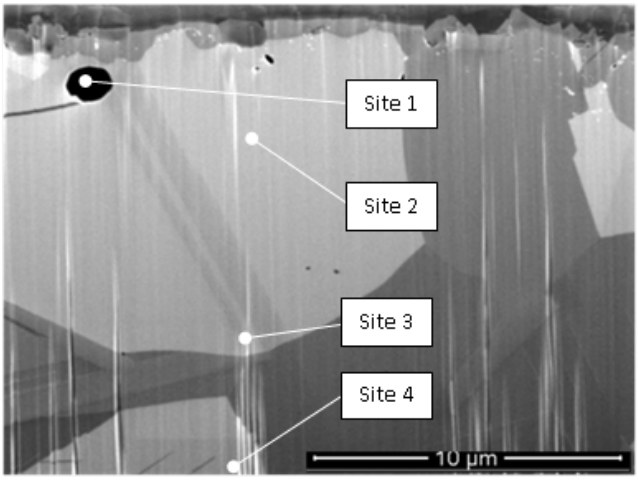

Figure 13 Cross section SEM image of Inconel 625 sample, 2500 hours testing (10000X)

In reference to Figure 13, four sites were chosen for EDX chemical composition analysis. Site 1, is located within the void seen in the upper left hand corner of the figure. The remaining three, labeled 2, 3 and 4 are located at successively deeper depths along the cross section into the parent material. A summary of the results is given in Table 6 below. The location at Site 1 reveals that molten salt has penetrated the void space, likely via a grain boundary. Site 2 results may indicate the presence of an oxide precipitate. Otherwise, the compositions are relatively uniform and consistent with the nominal alloy elements.

Table 6 EDX chemical analysis and resulting weight percentage of Inconel 625 sample cross section, 2500 hours testing

Site	O%	Na%	Nb%	Cl%	Cr%	Fe%	Ni%	Mo%
1	0.43	7	0.4	3.7	19.1	1.4	64.6	2.4

2	30.57	-	1.2	-	18.4	1.5	72.7	5.6
3	3.7	-	1.2	0.2	20.7	1.3	71.5	5.2
4	0.35	-	1.2	-	19.1	1.4	71	5.1

Conclusions

The corrosion process for both SS 316L and Inconel 625 material switched from an initial localized attack to a more uniform type, with neither sample having suffered severe damage even after 2500 hours. Undesirable intergranular grain boundary attack is found to have penetrated to a depth of just 1-2 μm. The corrosion rates appear to slow significantly after an initial stage, with the Inconel 625 showing an advantage in low corrosion activity in the long term. Both materials show promise for good compatibility with the NaF/NaCl eutectic salt mixture within a sealed system where excess water and oxygen is minimized. The testing conducted deviates from the actual operating conditions of the TES system in terms of thermal cycling. However, the results should be sufficient to guide material selection for proof of concept hardware.

ACKNOWLEDGMENTS

The authors would like to thank Bruce Arey at Environmental Molecular Sciences Laboratory at Pacific Northwest National Laboratory (PNNL) for his technical support, Sandia National Laboratories for its technical support, and the U.S. Department of Energy's Golden Field Office for its financial and technical support.

REFERENCES

[1] Mancini, T., et al., "Dish-Stirling Systems: An Overview of Development and Status", *Journal of Solar Energy Engineering,* May 2003, Vol. 125(2)

[2] Stine, W.B., Diver, R., "A Compendium of Solar Dish-Stirling Technology", Sandia National Laboratories, SAND93-7026 UC-236, January 1994

[3] Schreiber, J.G., "Summary of Stirling Convertor Testing at NASA Glenn Research Center", NASA/TM-2006-214429, June 2007

[4] Lide, D.R., *CRC Handbook of Chemistry and Physics, 79th Ed.,* 1999

[5] Mamantov, G., et al., *Molten Salt Chemistry- An Introduction and Selected Applications,* NATO Science Series C: Mathematical and Physical Sciences, 1987, Vol. 202

[6] Grimes, W.R., *Nuclear Application and Technology,* p137, 1970, Vol. 8(2)

[7] Luo, A.; Jacobson, D.L.; Ponnappan, R., *Journal of Material Engineering and Performance,* pp7-55, 1992, Vol. 16

[8] Khanna, A.S., *Introduction to High Temperature Oxidation and Corrosion,* ASM International, 2002